

# Correlation between the Mean Matter Density and the Width of the Saturated Ly $\alpha$ Absorption

Hu Zhan<sup>\*</sup>

*Department of Physics, University of Arizona, Tucson, AZ 85721, USA*

30 October 2018

## ABSTRACT

We report a scaling of the mean matter density with the width of the saturated Ly $\alpha$  absorptions. This property is established using the “pseudo-hydro” technique (Croft et al. 1998). It provides a constraint for the inversion of the Ly $\alpha$  forest, which encounters difficulty in the saturated region. With a Gaussian density profile and the scaling relation, a simple inversion of the simulated Ly $\alpha$  forests shows that the one-dimensional mass power spectrum is well recovered on scales above  $2 h^{-1}\text{Mpc}$ , or roughly  $k \lesssim 0.03 \text{ km}^{-1}\text{s}$ , at  $z = 3$ . The recovery underestimates the power on small scales, but improvement is possible with a more sophisticated algorithm.

**Key words:** cosmology: theory – large-scale structure of universe – quasars: absorption lines

## 1 INTRODUCTION

The Ly $\alpha$  forest has offered a unique way to study the large-scale structure of the universe at high redshifts. It is based on the theory that the Ly $\alpha$  forest is a result of the absorptions of quasar continuum by the diffusely distributed and photoionized intergalactic medium (IGM), and the IGM traces the density of the underlying mass field on scales larger than the Jeans length (Bi 1993; Cen et al. 1994; Bi et al. 1995; Petitjean et al. 1995; Viel et al. 2002). In other words, the baryon density in Ly $\alpha$  absorption systems is roughly proportional to the matter density, when  $\rho \lesssim 10$  (Bi & Davidsen 1997; Gnedin & Hui 1998; Zhang et al. 1998).

To extract the baryon density  $\rho_b$  or the mass density  $\rho$ , one may invert the transmitted flux  $F$  of the Ly $\alpha$  forest using

$$F = e^{-\tau} \simeq e^{-A\rho_b^\beta} \simeq e^{-A\rho^\beta}, \quad (1)$$

where:  $\tau$  is the Ly $\alpha$  optical depth;  $A$  depends on the temperature of IGM, the HII photoionization rate, and redshift (Rauch et al. 1997; Croft et al. 1998); and  $\beta$ , related to equation of state of the IGM (Hui & Gnedin 1997), is in the range 1.6–1.8 (Croft et al. 1999). The densities are in units of their corresponding cosmic mean density, and so the overdensity  $\delta = \rho - 1$ .

When the density is high enough, the spectrum is saturated, i.e.  $F \simeq 0$ . With noises and uncertainties in the spectrum, the direct inversion using equation (1) is very unreliable in the saturated region. Despite the difficulty, methods of direct inversion are systematically developed, for ex-

ample, with Lucy’s method by Nusser & Haehnelt (1999), and with Bayesian method for a three-dimensional inversion by Pichon et al. (2001). One may also use higher order lines to recover the optical depth and the underlying density (Cowie & Songaila 1998; Aguirre et al. 2002), even though the contamination by lower order lines needs to be carefully removed. Once the cosmic density field is obtained, many statistics, such as the mass power spectrum, can be measured.

Another approach is taken by Croft et al. (1998, 1999, 2002) to map the mass power spectrum directly from the flux power spectrum of the Ly $\alpha$  forest without an inversion. Thus the saturation problem is avoided. However, a close examination of the Fourier transform of equation (1) shows that powers on different scales are mixed by the non-linear density–flux relation (see Section 4). The mixing depends on the underlying density field, and it is hard to predict analytically.

If the inversion is necessary, a proper treatment in the saturated region has to be developed. In many physical systems, sizes are often correlated with other quantities such as masses and densities. For example, more massive stars or dark matter haloes have larger sizes, but lower mean densities (Binney & Merrifield 1998; Navarro et al. 1996). One may expect a similar trend for the saturated Ly $\alpha$  absorption. On the contrary, the mean density is found to increase with the width of saturation. This is due to the fact that the IGM is very diffuse and far from virialization, while the other objects mentioned are the opposite.

This paper is organised as follows. Section 2 presents the scaling relation. A simple inversion with the scaling is tested in Section 3 for both the one-dimensional mass power

<sup>\*</sup> Email: zhanhu@physics.arizona.edu

spectrum and the one-point distribution function. Section 4 examines the mapping between the mass power spectrum and the flux power spectrum. The discussion and conclusions are given in Section 5. Unless addressed otherwise, the power spectra below are implicitly one-dimensional.

## 2 THE SCALING

Neglecting the probability that two physically separate absorption systems fall in the same redshift coordinate, one can associate a saturated absorption in the Ly $\alpha$  forest with a single high density region. If we assume further that there is no substructure present, and the IGM evolves more or less the same way everywhere, then the size of the saturated region has to be tightly correlated with its mean density (Schaye 2001). In reality, the neglected elements above and uncertainties elsewhere will introduce a spread to the correlation.

### 2.1 Simulated Ly $\alpha$ Forest

It is demonstrated by various hydrodynamical simulations (Bi & Davidsen 1997; Gnedin & Hui 1998; Zhang et al. 1998; Bryan et al. 1999; Davé et al. 1999, 2001) that the baryon density, the H I column density, and the IGM temperature correlate well with the underlying dark matter density for  $\rho \lesssim 10$ . This leads to the useful “pseudo-hydro” technique (Croft et al. 1998) for simulating the Ly $\alpha$  forest with collisionless N-body simulations instead of hydrodynamical simulations. Basically it draws the line-of-sight (LOS) dark matter density in redshift space from N-body simulations, and then converts the density to flux using equation (1).

One may have concerns about the Jeans length, below which the pseudo-hydro technique may not be applicable. The comoving Jeans length  $L_J$  is

$$L_J = \frac{c_s(1+z)}{\sqrt{G\rho}} = \sqrt{\frac{8\pi\gamma k_B T}{3\mu m_p H_0^2 \Omega \rho(1+z)}} \\ = 440 \text{ } h^{-1} \text{ kpc } T_4^{1/2} [\Omega \rho(1+z)]^{-1/2}, \quad (2)$$

where  $c_s$  is the speed of sound,  $G$  is the gravitational constant,  $\gamma = 5/3$  is the ratio of specific heats,  $k_B$  is the Boltzman constant,  $T$  is the temperature,  $\mu = 0.59$  is the mean molecular weight,  $m_p$  is the proton mass,  $H_0 = 100 \text{ km s}^{-1} \text{ Mpc}^{-1}$ ,  $\Omega$  is the matter density in units of the critical density at present, and  $T_4 \simeq 1.5$  is the temperature in units of  $10^4 \text{ K}$ . It is understood that the first  $\rho$  in equation (2) is the actual density, while the rest are densities in units of the cosmic mean density. For the low-density cold dark matter (LCDM) model at  $z = 3$  and  $\rho = 1$ ,  $L_J = 490 \text{ } h^{-1} \text{ kpc}$ . The Jeans length suggests that the smallest scale we can analyse reliably without hydrodynamical simulations is  $0.5 \text{ } h^{-1} \text{ Mpc}$ . However, saturated regions usually have  $10 \gtrsim \rho \gtrsim 5$  (see Fig. 1), and the temperature scales with the density as  $T \propto \rho^\alpha$  with  $\alpha = 0.3\text{--}0.6$  (Hui & Gnedin 1997), so the Jeans length is reduced by a factor of 1.4–2.2 in those regions. In addition, Gnedin & Hui (1998) point out that the actual linear filtering scale is 1.5–2.5 times smaller than the Jeans length at  $z = 3$ , such that baryons trace the dark matter on scales even half of  $L_J$ . Hence, the pseudo-

**Table 1.** Parameters of the N-body simulations.

Model	$\Omega$	$\Lambda$	$h$	$\Gamma$	$\sigma_8$
LCDM	0.3	0.7	0.7	0.21	0.85
OCDM	0.3	0	0.7	0.21	0.85
SCDM	1.0	0	0.5	0.5	0.67
TCDM	1.0	0	0.5	0.25	0.60

$h$  is the Hubble constant in units of  $100 \text{ km s}^{-1} \text{ Mpc}^{-1}$ .

$\Gamma$  is the shape parameter in the power spectrum.

$\sigma_8$  is the r.m.s. density fluctuation within a radius of  $8 \text{ } h^{-1} \text{ Mpc}$ .

hydro technique is sufficient for the analysis above the scale of  $200 \text{ } h^{-1} \text{ kpc}$ .

A standard particle-particle-particle-mesh (P<sup>3</sup>M, Hockney & Eastwood 1981) code developed by Jing & Fang (1994) is used to evolve  $128^3$  dark matter particles in a cubic box of  $12.8 \text{ } h^{-1} \text{ Mpc}$  (comoving) each side. The initial power spectrum is given by the fitting formula from Bardeen et al. (1986). The model parameters are listed in Table 1. All the models start from  $z = 15$ , and stop at  $z = 3$  in 950 steps.

The parameter  $A$  in equation (1) is chosen to fit the mean flux  $\langle F(z) \rangle = \exp[-\tau(z)]$ , where  $\tau(z) = 0.0032(1+z)^{3.37}$  for  $z = 3\text{--}4$  (Kim et al. 2002). This mean flux formula is consistent with other observations (Lu et al. 1996; Rauch et al. 1997; McDonald et al. 2000). We extrapolate the mean flux up to  $z = 4.5$ , which is not critical to the analysis in Section 2.2, but is nevertheless supported by simulations (Riediger et al. 1998). The constant  $\beta$  in equation (1) is set to 1.6. Four samples of the Ly $\alpha$  forest are shown in Fig. 1. They are drawn from the LCDM simulation at  $z = 3$ . The corresponding LOS densities are plotted along with the fluxes. It is evident that most of the Ly $\alpha$  lines arise where  $\rho \lesssim 10$ .

### 2.2 The Scaling

We define the width  $w$  of the saturation as the distance between the two points that bracket the absorption at a given threshold flux level  $\eta$ . In other words, it is the width of a region in which  $F < \eta$ . Since the flux  $F$  in the saturated region is dominated by noise, one should set the threshold above the noise level. Within a reasonable range of spectral quality, we choose the threshold  $\eta = 0.03$  and  $0.10$  for the tests below.

Once the width is determined, the mean density  $\bar{\rho}$  can be readily calculated from the corresponding LOS density field. Since the density and the flux are assigned only on grid points, interpolation is needed to find  $w$  and  $\bar{\rho}$ . Fig. 2 shows the scaling relation for the LCDM model at  $z = 3$ . It clearly demonstrates that  $\bar{\rho}$  increases with  $w$ . Furthermore, the correlation is reasonably tight for narrow saturations. Notice that the trend lines are obtained by fitting only the data with  $w \leq 2 \text{ } h^{-1} \text{ Mpc}$ , because wider saturations are very rare as compared to the rest.

The  $\bar{\rho}$ – $w$  relation is well fitted by

$$\bar{\rho} = \rho_0 + a (w/h^{-1} \text{ Mpc})^b. \quad (3)$$

The term  $\rho_0$  sets a baseline for the scaling, because the matter density is non-vanishing even if there is no saturation.

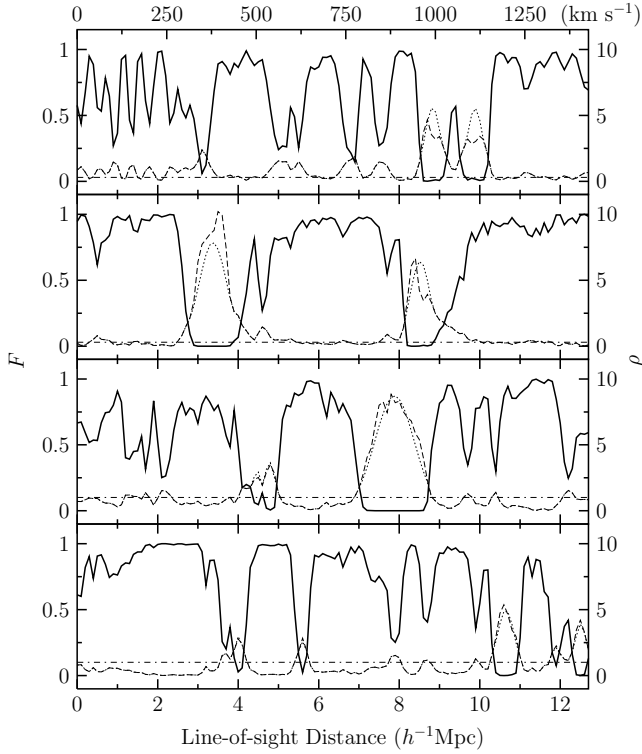


**Figure 1.** Samples of the simulated Ly $\alpha$  forest from the LCDM model at  $z = 3$ . The solid lines are the flux  $F$ , the dashed lines are the matter density  $\rho$ , the dotted lines are the recovered density, and the horizontal dash-dotted lines indicate the threshold flux level  $\eta = 0.03$  (see Section 3) in the upper 2 panels, and  $\eta = 0.10$  in the lower 2 panels. The scale of the densities, in units of cosmic mean density, is indicated on the right axis. The flux and the density are both presented in redshift space.

**Table 2.** Parameters in the fitting  $\bar{\rho} = \rho_0 + a (w/h^{-1}\text{Mpc})^b$  for the LCDM model.

$z$	$\eta$	$\rho_0$	$a$	$b$
3	0.03	1.93	3.85	0.545
	0.10	1.39	3.39	0.564
4.5	0.03	0.11	2.78	0.455
	0.10	0.24	2.04	0.556

The parameter  $a$  is a scaling factor, which reflects the overall amplitude of the density fluctuation, and the exponent  $b$  is more or less determined by the nature of hierarchical clustering. The width  $w$  is in units of  $h^{-1}\text{Mpc}$ . Table 2 lists the values for LCDM model at  $z = 3$  and 4.5. The reason why  $\rho_0$  decreases with redshift is that the universe is more uniform early on, so that even low density regions have to absorb a substantial amount of Ly $\alpha$  flux to produce the low mean flux. This is possible because the neutral fraction of the IGM at  $z = 4.5$  is higher than that at  $z = 3$ . As the universe evolves, the density fluctuation grows stronger and stronger, and the scaling factor  $a$  becomes larger and larger. The exponent  $b$  has changed little over  $z = 3$ –4.5. The parameters also show a dependence on the threshold flux  $\eta$ , because  $\eta$  sets the threshold density  $\rho_\eta$ , above which the  $\bar{\rho}$ – $w$  relation is explored.

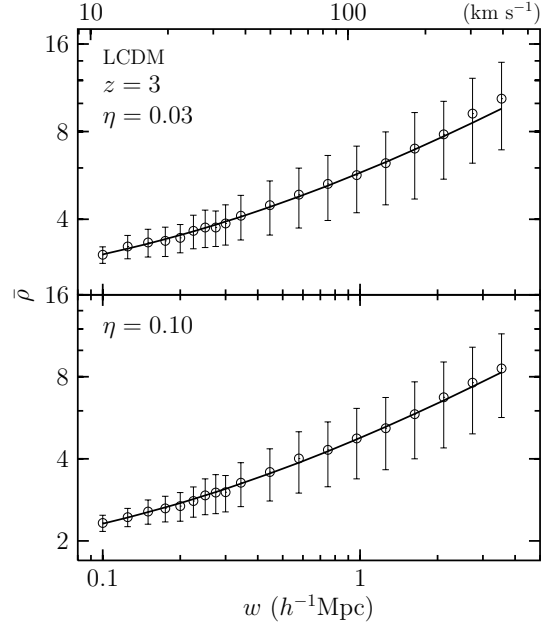


**Figure 2.** The correlation between the mean density  $\bar{\rho}$  and the width  $w$  of the saturated region in the Ly $\alpha$  forest. The trend lines fit the data well beyond  $2 h^{-1}\text{Mpc}$ , even though they are obtained by fitting only the data with  $w \leq 2 h^{-1}\text{Mpc}$ . The data above  $0.3 h^{-1}\text{Mpc}$  are binned in logarithmic intervals for readability. Similar treatment applies to Figs 4, 5, 6, and 9 as well.

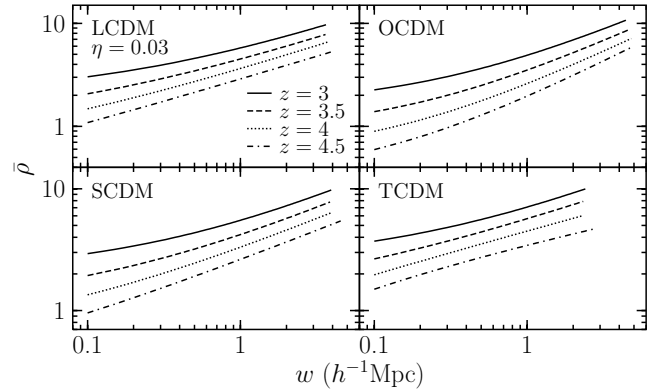


**Figure 3.** The best-fittings of the  $\bar{\rho}$ – $w$  relation for the 4 models at  $z = 3$ –4.5. The threshold  $\eta = 0.03$ . The parameters are obtained by fitting the saturations with  $w \leq 2 h^{-1}\text{Mpc}$ .

Fig. 3 shows the evolution of the  $\bar{\rho}$ – $w$  relation for the 4 models. The difference between models is mostly due to the amplitude of fluctuations – in other words, the power spectrum.

### 2.3 The Physics

The  $\bar{\rho}$ – $w$  relation is analogous – but not completely equivalent – to the curve of growth (e.g. Press & Rybicki 1993), which studies the correlation between the HI column density  $N_{\text{HI}}$  and the equivalent width  $W$  of Ly $\alpha$  absorptions. The similarity is as follows. The width  $w$  is approximately the same as  $W$ , and the mean matter density  $\bar{\rho}$  is proportional to  $w^{-1}N_{\text{HI}}$  if  $\rho \propto \rho_b$  holds true. Since  $N_{\text{HI}} \propto W$  at small

values of  $W$ , it is not surprising to see  $\bar{\rho}$  grow slowly, i.e.  $d \ln \bar{\rho} / d \ln w \sim 0$ , for small  $w$ .

On the other hand, the  $\bar{\rho}$ - $w$  relation addresses saturated absorptions where, according to the curve-of-growth analysis,  $W$  is almost a constant independent of the HI column density. Therefore,  $\bar{\rho}$  would have risen steeply against  $w$ , i.e.  $b \gg 1$ . This apparent inconsistency arises from the cosmological context, because the width  $w$  is determined not only by  $N_{\text{HI}}$  but also by the physical extent of the (relatively) dense region through Hubble expansion and peculiar velocities.

Although it is not obvious why  $b$  is less than unity, we can make an order-of-magnitude estimate using the density profile  $\rho(r) \propto r^{-1}$  from a spherical self-similar infall. We modify the profile to avoid the singularity at  $r = 0$  by adding a smoothing length  $\epsilon$ , so that  $\rho(r) \propto (r^2 + \epsilon^2)^{-1/2}$ . The mean density within the radius  $R$ , at which  $\rho = \rho_\eta$ , is

$$\bar{\rho}(R) = \frac{3}{R^3} \int_0^R \rho(r) r^2 dr = \frac{3\rho_\eta \sqrt{R^2 + \epsilon^2}}{2R^3} \times \left[ R \sqrt{R^2 + \epsilon^2} + \epsilon^2 \log \left( \frac{\epsilon}{R + \sqrt{R^2 + \epsilon^2}} \right) \right]. \quad (4)$$

From equation (4), one gets an estimate  $b \sim d \ln \bar{\rho} / d \ln R = 0.39, 0.42$ , and  $0.43$  for  $\epsilon = 0.2, 0.3$ , and  $0.4 h^{-1} \text{Mpc}$  respectively at  $R = 2 h^{-1} \text{Mpc}$ . The same quantity for the  $\bar{\rho}$ - $w$  relation is  $d \ln \bar{\rho} / d \ln w = 0.41$ , where we have used the parameters of the LCDM model at  $z = 3$  with  $\eta = 0.03$  (see Table 2). It should be stressed that the  $\rho(r) \propto r^{-1}$  profile is not quite justified for the IGM at  $z = 3$ , and without any modification, it gives the same mean density within the boundary  $\rho = \rho_\eta$  regardless the size of the system, i.e.  $b = 0$ . Therefore, equation (4) is not expected to give a fair approximation of the  $\bar{\rho}$ - $w$  relation.

### 3 INVERSION WITH A GAUSSIAN DENSITY PROFILE

If the flux level is above the threshold, equation (1) can be used to find the density. When it is below the threshold, one must provide a density profile that matches  $\bar{\rho}(w)$  and  $\rho_\eta$  to fill in the missing information in the saturation.

While the density profile is worth studying in its own right, we simply choose the Gaussian profile

$$\rho(s) = \frac{B}{\sigma \sqrt{2\pi}} \exp \left[ -\frac{1}{2} \left( \frac{s - s_0}{\sigma} \right)^2 \right], \quad (5)$$

where  $s$  is the coordinate in redshift space,  $s_0$  is the centre of the saturation, and  $B$  and  $\sigma$  are solved simultaneously from

$$\bar{\rho}(w) = \frac{1}{w} \int_{s_0 - w/2}^{s_0 + w/2} \rho(s) ds = \frac{B}{w} \text{erf} \left( \frac{1}{2\sqrt{2}} \frac{w}{\sigma} \right), \quad (6)$$

$$\rho_\eta = \rho(s_0 \pm w/2) = \frac{B}{\sigma \sqrt{2\pi}} \exp \left[ -\frac{1}{8} \left( \frac{w}{\sigma} \right)^2 \right],$$

where  $\text{erf}(x)$  is the error function. The Gaussian profile has the advantage that it does not introduce any artificial power on small scales. However, it is arguable that the right amount of small-scale power should be added through the profile, and so a more realistic profile may be needed.

The recovered LOS densities with  $\eta = 0.03$  and  $\eta = 0.10$

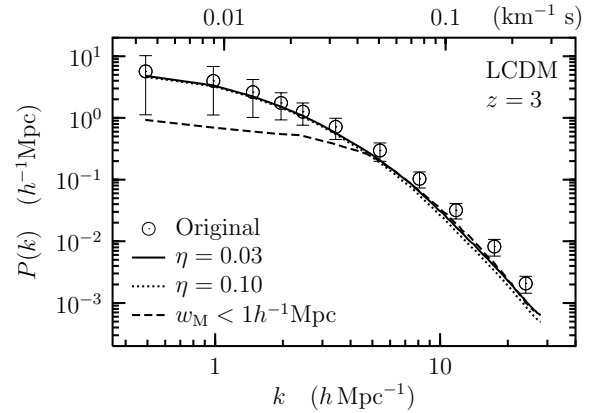


**Figure 4.** The power spectra of original densities and recovered densities in redshift space. Circles include all LOS densities from the N-body simulation, and the dashed line contains only the ones that have a maximum width of saturation  $w_M < 1 h^{-1} \text{Mpc}$ . The recovered densities are inverted from fluxes with thresholds  $\eta = 0.03$  (solid line) and  $\eta = 0.1$  (dotted line). The error bars are  $1\sigma$  dispersions among 610 groups, each of which consists of 20 LOS densities. The error bars of the recovered densities, which are not plotted, are comparable to that of the original densities.

are shown along with the four original LOS densities and fluxes in Fig. 1. Since a universal density profile is employed in the inversion, the recovered densities do not necessarily match the original densities.

To assess the statistical quality of the inversion, we plot in Fig. 4 the original and the recovered mass power spectra of the LCDM model with different flux thresholds. Other models are shown in Fig. 5. The recovered power spectrum agrees well with the original power spectrum on large scales ( $k \lesssim 3 h \text{Mpc}^{-1}$ ), but it is underestimated on smaller scales, where the Gaussian profile essentially has no power. The signal to noise ratio, or the threshold flux, has little influence on large scales, but a low noise level does slightly improve the recovery on small scales.

For comparison, we show in Figs 4 and 5 the original power spectrum of the LOS densities that have a maximum width of saturation  $w_M < 1 h^{-1} \text{Mpc}$ . This is equivalent to removing – or giving less weight to – the saturated regions when one measures the power spectrum. It is seen that the saturated regions are very important to scales  $\gtrsim 2 h^{-1} \text{Mpc}$ , while the unsaturated regions give a good estimate of the small-scale power. Thus one may improve the recovery of power spectrum as follows. First, invert the Ly $\alpha$  forest with equation (1) and the  $\bar{\rho}$ - $w$  relation. Second, do the inversion after removing the saturated regions. Finally, the best-estimate of the power spectrum is just the common envelope of the power spectra of the two recovered densities.

Fig. 3 indicates that the  $\bar{\rho}$ - $w$  relation varies from model to model. Thus it is necessary to check if the recovery is sensitive to  $\bar{\rho}(w)$  – in other words, if it is model dependent. In Fig. 6 we plot the power spectra of LCDM densities recovered with  $\bar{\rho}_O(w)$  and  $\bar{\rho}_T(w)$  from open cold dark matter (OCDM) and tilted cold dark matter (TCDM) models respectively. It seems that by boosting  $\bar{\rho}(w)$  a small amount [ $\bar{\rho}_T(w)$  lies a little higher than  $\bar{\rho}_L(w)$ ], one gets even better estimate of the power spectrum on small scales. However, lowering  $\bar{\rho}(w)$  could underestimate the power by a factor of

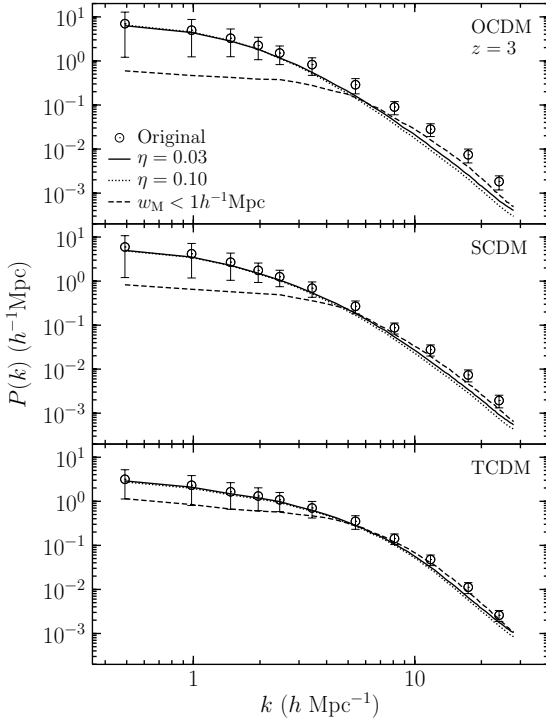


**Figure 5.** The same as Fig. 4, but for OCDM, SCDM, and TCDM models.

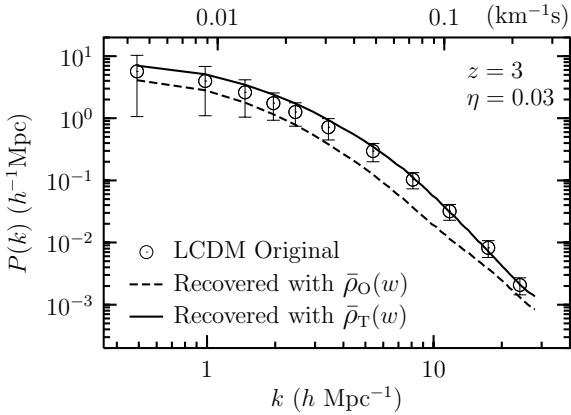


**Figure 6.** The same as Fig. 4, except that the fluxes are drawn from the LCDM simulation, while the densities are recovered with  $\bar{\rho}$ - $w$  relations from OCDM and TCDM simulations.

2 on large scales, and even more on small scales. The effect of this model dependence could be reduced with the constraint on small scales, since it is possible to recover the small-scale power well by removing the saturations.

Fig. 7 tests a different statistics – the one-point distribution function for the LCDM model. It is evident that the Gaussian profile leads to a drop of the probability at high densities. In other words, it statistically reduces the heights of density peaks.

#### 4 MAPPING THE POWER SPECTRA

It seems that the inversion is no longer needed at least for determining the mass power spectrum if one establishes a di-

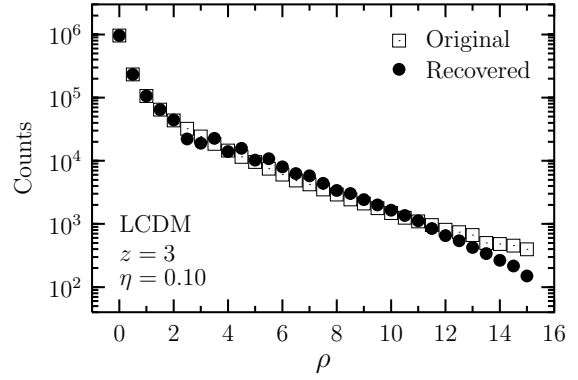


**Figure 7.** The one-point distribution function of the recovered densities (filled circles) and that of the original densities (open squares).

rect mapping between the flux and the mass power spectra (Croft et al. 2002). It is shown that given a set of cosmological parameters, there is a statistical mapping, which reliably recovers the mass power spectrum from the flux power spectrum (Gnedin & Hamilton 2002), even though the mapping is model dependent.

The physical links between the three-dimensional linear mass power spectrum  $\mathcal{P}_L(k)$  and the flux power spectrum can be summarised by the flowchart:

$$\mathcal{P}_L(k) \longrightarrow \mathcal{P}_{NL}(k) \longrightarrow \mathcal{P}_{NL}^S(\mathbf{k}) \longrightarrow P(k) \xrightarrow{d^2(k)} P_F(k),$$

where  $\mathcal{P}_{NL}(k)$  is the 3D non-linear mass power spectrum (Peacock & Dodds 1996; Taylor & Hamilton 1996),  $\mathcal{P}_{NL}^S(\mathbf{k})$  is  $\mathcal{P}_{NL}(k)$  in redshift-space (Kaiser 1987; Peacock 1999; Zhan & Fang 2003), and  $d^2(k) = P_F(k)/P(k)$ . Notice that  $\mathcal{P}_{NL}^S(\mathbf{k})$  is anisotropic. We show in Fig. 8 that the non-linear evolution and the redshift distortion are significant at  $z = 3$ . The fact that the departure from linear evolution is very similar in both large and small box simulations indicates that such departure is real, and the cosmic density field has already gone non-linear below  $10 h^{-1}\text{Mpc}$  at  $z = 3$  (see also Zhan et al. 2001; Pichon et al. 2001). The angularly averaged 3D power spectrum  $\mathcal{P}_{NL}^S(k)$  does not give a complete view of the difference between the real-space power spectrum and redshift-space power spectrum, but it does show that peculiar velocities boost the power on large scales and reduce it substantially on small scales. A two-dimensional projection of  $\mathcal{P}_{NL}^S(\mathbf{k})$  can be found in Peacock et al. (2001).

In contrast, the mapping in Croft et al. (2002) follows a simplified path:

$$\mathcal{P}_L(k) \longrightarrow P_L(k) \xrightarrow{b^2(k)} P_F(k),$$

where  $P_L(k) = (2\pi)^{-1} \int_k^\infty \mathcal{P}_L(y) y dy$  (Kaiser & Peacock 1991), and  $b^2(k) = P_F(k)/P_L(k)$ . Since  $\mathcal{P}_{NL}^S(\mathbf{k})$  is anisotropic,  $P(k)$  and  $\mathcal{P}_{NL}^S(\mathbf{k})$  do not follow the same integral. Given a one-dimensional density field in redshift space at  $z = 3$ , one can only measure  $P(k)$ , and so  $P_L(k)$  is not observable unless the density field is linear on all scales and no peculiar velocity is present. In other words,  $P(k)$  is directly connected to  $P_F(k)$ , while  $P_L(k)$  is not.

Around the cosmic mean matter density, i.e.  $|\delta| \ll 1$ , equation (1) is approximately

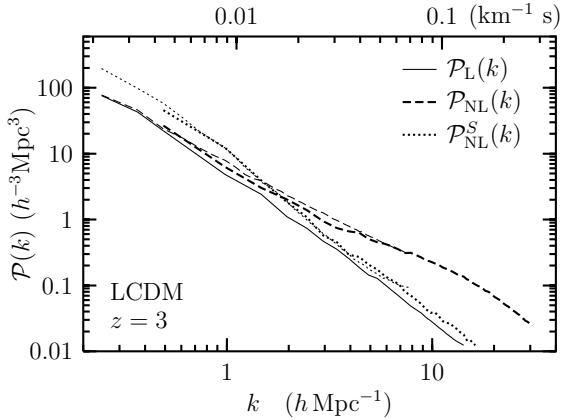


**Figure 8.** The 3D power spectrum of the LCDM model at  $z = 3$ . The dashed lines are the real-space power spectra, the dotted lines are the redshift-space power spectra averaged over solid angles, and the thin solid line is the initial power spectrum (at  $z = 15$ ) evolved to  $z = 3$  by linear theory. The thin dashed line and the thin dotted line are from an additional simulation with the same parameters as the LCDM model except that the box is  $51.2 h^{-1}\text{Mpc}$  each side.

$$F(s) \simeq e^{-A} - A\beta e^{-A}\delta(s), \quad (7)$$

where we have included the dependence on the redshift coordinate  $s$  explicitly. It is seen in the linearized equation (7) that the Fourier modes of the flux are proportional to those of the overdensity when  $k \neq 0$ . Hence, the flux power spectrum is proportional to the mass power spectrum

$$P_F(k) \simeq A^2 \beta^2 e^{-2A} P(k), \quad k \neq 0. \quad (8)$$

Caution should be taken when using equation (7), because it is valid only if one smoothes the Ly $\alpha$  forest over large scales (see, for example, Zhan et al. 2001; Zhan & Fang 2002).

It is obvious from equation (1) and Fig. 1 that the condition  $|\delta(s)| \ll 1$  is never met where  $F \simeq 1$  or  $F \simeq 0$ . Therefore, one has to include higher order terms of  $\delta(s)$ . Taking the simplest case, in which  $\delta(s) = \sin(k_0 s)$  and only  $\delta^2(s)$  term is added to equation (7), one immediately finds that  $P_F(k)$  contains spurious power on the mode  $2k_0$  that  $P(k)$  does not contain. In general, the non-linear density-flux relation distorts, spreads, and mixes power in the cosmic density field over different scales in the flux power spectrum. Other sources of distortion originate from linear filtering (Gnedin & Hui 1998), line profile (see Gray 1992), and instrumentation. We do not focus on these effects, since they are well studied in the literature.

Fig. 9 shows the ratio  $b(k)$  and  $d(k)$ . The dispersion in  $d(k)$  is larger than that of  $b(k)$ , because both  $P_F(k)$  and  $P(k)$  contribute to the dispersion of  $d(k)$ , while  $b(k)$  receives only a single contribution from  $P_F(k)$ . Even so, the error propagation would cause a large scatter in determining  $P_L(k)$ . In fact, the scatter can be large enough that one would not be able to determine the cosmological model based only on the recovered  $P_L(k)$ . On the other hand, the model dependence of  $b(k)$  is strong enough, so that one may have to assume *a priori* the cosmological model to recover the mass power spectrum from the flux power spectrum. The difference among the models is not solely due to  $\sigma_8$ . For example, the standard cold dark matter (SCDM) model has a slightly higher  $\sigma_8$  than the  $\Lambda$ CDM model, so one would ex-

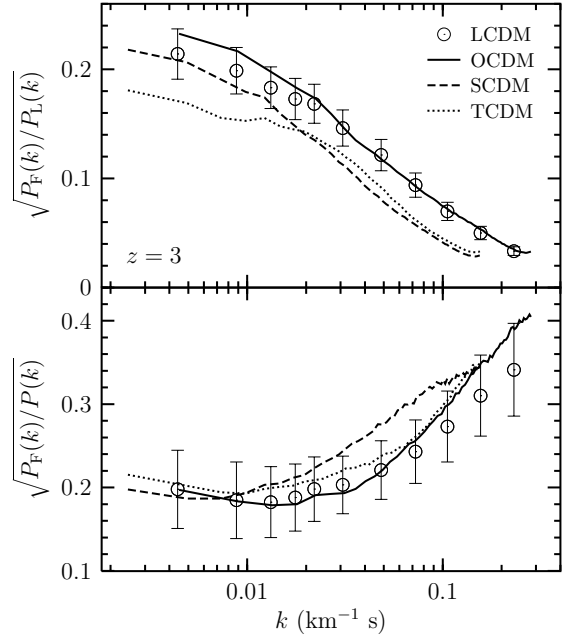


**Figure 9.** The ratio  $b(k) = \sqrt{P_F(k)/P_L(k)}$  (upper panel) and  $d(k) = \sqrt{P_F(k)/P(k)}$  (lower panel). The Ly $\alpha$  forests are divided into groups, each of which consists of 20 LOS samples. The power spectra are averaged within each group except  $P_L(k)$ , which is theoretical. The error bars of the LCDM model are  $1\sigma$  dispersions among 610 groups. Error bars of other models are comparable to that of the LCDM model.

pect  $b(k)$  of the SCDM model to have the same shape as that of the  $\Lambda$ CDM model but with a shift. This is not observed in Fig. 9, however. It is also evident from the behaviour of  $b(k)$  and  $d(k)$  that the power spectrum of the underlying density field  $P(k)$  is significantly lower than the linear mass power spectrum  $P_L(k)$  on scales  $k > 0.02 (\text{km s}^{-1})^{-1}$ . This is due mostly to the peculiar velocity, or redshift distortion.

## 5 DISCUSSION AND CONCLUSIONS

We have provided a scaling relation between the mean matter density and the width of the saturated Ly $\alpha$  absorptions. It has not been tested against variations of  $A$  or  $\beta$  [see equation (1)], because the  $\bar{\rho}$ - $w$  relation is the property of the density field, while changing  $A$  or  $\beta$  can only affect the width of the saturation, and consequently determines which part of the scaling to be measured. This is also why the  $\bar{\rho}$ - $w$  relation slightly depends on the threshold flux, below which the underlying density cannot be directly extracted from the flux.

The inversion with the  $\bar{\rho}$ - $w$  relation is able to recover the mass power spectrum fairly well on scales above  $2 h^{-1}\text{Mpc}$ , but underestimates the power on small scales due to the use of the Gaussian profile. An improvement is suggested based on the observation that the power spectrum, with saturations removed, recovers the small-scale power well. Thus, by combining both the  $\bar{\rho}$ - $w$  inversion and the result after removing the saturations, one could get a good estimate of the power spectrum on all scales.

The Gaussian profile does not preserve the high-density

tail of the one-point distribution function either. A more realistic density profile may improve the one-point distribution function, but the complication of substructures and peculiar velocities could result in only a small margin for improvement.

The  $\bar{\rho}$ - $w$  relation provides an important constraint to the inversion of the Ly $\alpha$  forest. To incorporate it in any inversion scheme, one needs to determine the  $\bar{\rho}$ - $w$  relation according to spectral resolution and noise. The threshold flux can be conveniently set to a small value above the noise level. That is why we have not added any noise in the simulations: noise outside the saturation can be routinely dealt with, while noise in the saturation, being below the threshold, does not matter.

The density is so far recovered in redshift space. The real-space density can be obtained iteratively (Nusser & Haehnelt 1999), and the real-space three-dimensional mass power spectrum can be recovered using matrix method (Hui 1999), or less rigorously by differentiation (Croft et al. 1998).

It is discussed in Section 2.1 that the pseudo-hydro technique is reliable above  $200 h^{-1}\text{kpc}$  at  $z = 3$ . This means that while the bulk of our analysis is valid, the details below  $200 h^{-1}\text{kpc}$  may be subject to hydrodynamic effects. In the future, we will put the  $\bar{\rho}$ - $w$  relation on test using hydrodynamical simulations.

Finally we find that the non-linear evolution and redshift distortion have significantly changed the mass power spectrum at  $z = 3$ . Therefore, the linear mass power spectrum  $P_L(k)$  is not directly observable, and it is substantially larger than the mass power spectrum  $P(k)$  on scales  $k > 0.02 (\text{km s}^{-1})^{-1}$  at  $z = 3$ .

## ACKNOWLEDGMENTS

HZ thanks D. Burstein, R. Davé, D. Eisenstein, and L.Z. Fang for helpful discussions. HZ also thanks the referee for comments that help to improve the paper.

## REFERENCES

- Aguirre A., Schaye J., Theuns T., 2002, *ApJ*, 576, 1  
 Bardeen J.M., Bond J.R., Kaiser N., Szalay A.S., 1986, *ApJ*, 304, 15  
 Bi H.G., 1993, *ApJ*, 405, 479  
 Bi H.G., Davidsen A.F., 1997, *ApJ*, 479, 523  
 Bi H.G., Ge J., Fang L.Z., 1995, *ApJ*, 452, 90  
 Binney J., Merrifield M., 1998, *Galactic Astronomy*, Princeton Univ. Press, Princeton, NJ, p. 110  
 Bryan G.L., Machacek M., Anninos P., Norman M.L., 1999, *ApJ*, 517, 13  
 Cen R., Miralda-Escudé J., Ostriker J.P., Rauch M., 1994, *ApJ*, 437, L9  
 Cowie L.L., Songaila A., 1998, *Nature*, 394, 44  
 Croft R.A.C., Weinberg D.H., Katz N., Hernquist L., 1998, *ApJ*, 495, 44  
 Croft R.A.C., Weinberg D.H., Pettini M., Hernquist L., Katz N., 1999, *ApJ*, 520, 1  
 Croft R.A.C., Weinberg D.H., Bolte M., Burles S., Hernquist L., Katz N., Kirkman D., Tytler D., 2002, *ApJ*, 581, 20  
 Davé R., Hernquist L., Katz N., Weinberg D.H., 1999, *ApJ*, 511, 521  
 Davé R., Cen R., Ostriker J.P., Bryan G.L., Hernquist L., Katz N., Weinberg D.H., Norman M.L., O'Shea B., 2001, *ApJ*, 552, 473  
 Gnedin N.Y., Hamilton A.J.S., 2002, *MNRAS*, 334, 107  
 Gnedin N.Y., Hui L., 1998, *MNRAS*, 296, 44  
 Gray D., 1992, *The Observation and Analysis of Stellar Photospheres*, Cambridge Univ. Press, New York  
 Hockney R.W., Eastwood J.W., 1981, *Computer Simulation Using Particles*, McGraw-Hill, New York  
 Hui L., 1999, *ApJ*, 516, 519  
 Hui L., Gnedin N.Y., 1997, *MNRAS*, 292, 27  
 Jing Y.P., Fang L.Z., 1994, *ApJ*, 432, 438  
 Kaiser N., 1987, *MNRAS*, 227, 1  
 Kaiser N., Peacock J.A., 1991, *ApJ*, 379, 482  
 Kim T.-S., Carswell R.F., Cristiani S., D'Odorico S., Giallongo E., 2002, *MNRAS*, 335, 555  
 Lu L., Sargent W.L.W., Womble D.S., Takada-Hidai M., 1996, *ApJ*, 472, 509  
 McDonald P., Miralda-Escudé J., Rauch M., Sargent W.L.W., Barlow T.A., Cen R., Ostriker J.P., 2000, *ApJ*, 543, 1  
 Navarro J.F., Frenk C.S., White S.D.M., 1996, *ApJ*, 462, 563  
 Nusser A., Haehnelt M., 1999, *MNRAS*, 303, 179  
 Peacock J.A., 1999, *Cosmological Physics*, Cambridge Univ. Press, Cambridge  
 Peacock J.A., Dodds S.J., 1996, *MNRAS*, 280, L19  
 Peacock J.A. et al., 2001, *Nature*, 410, 169  
 Petitjean P., Mückel J.P., Kates R.E., 1995, *A&A*, 295, L9  
 Pichon C., Vergely J.L., Rollinde E., Colombi S., Petitjean P., 2001, *MNRAS*, 326, 597  
 Press W.H., Rybicki G.B., 1993, *ApJ*, 418, 585  
 Rauch M., Miralda-Escudé J., Sargent W.L., Barlow T.A., Weinberg D.H., Hernquist L., Katz N., Cen R., Ostriker J.P., 1997, *ApJ*, 489, 7  
 Riediger R., Petitjean P., Mückel J.P., 1998, *A&A*, 329, 30  
 Schaye J., 2001, *ApJ*, 559, 507  
 Taylor A.N., Hamilton A.J.S., 1996, *MNRAS*, 282, 767  
 Viel M., Matarrese S., Mo H.J., Haehnelt M.G., Theuns T., 2002, *MNRAS*, 329, 848  
 Zhan H., Fang L.Z., 2002, *ApJ*, 566, 9  
 Zhan H., Fang L.Z., 2003, *ApJ*, 585, 12  
 Zhan H., Jamkhedkar P., Fang L.Z., 2001, *ApJ*, 555, 58  
 Zhang Y., Meiksin A., Anninos P., Norman M.L., 1998, *ApJ*, 495, 63